VISUALISATION OF THE FLOW OVER A DISC-WING

J. R. Potts[1], W. J. Crowther[2]

Keywords: disc-wing, rotating bodies, smoke wire, laser illumination, fluorescence

ABSTRACT

An experimental investigation into the flow characteristics of a disc-wing has been carried out in a low speed wind tunnel over a flow speed range of 0 to 20 m/s. The disc-wing considered has an axi-symmetric, approximately elliptic cross-section and hollowed out underside cavity. The aim of this research was to gain an understanding of the complex three-dimensional flow structures, in order to identify regions receptive to flow control technologies such as vortex generators or synthetic (massless) jets. Flow visualisation techniques including surface paint and smoke wire methods have been utilised to determine the position and form of surface flow structures.

NOMENCLATURE

AdvR	Advance ratio ($\Omega\pi D / V$)	Re	Reynolds number (based on D)
*A*R	Aspect ratio	T	Disc thickness (m)
cg	centre of gravity	V	Wind velocity (ms^{-1})
cp	centre of pressure	L,M,N	Rolling, pitching, yawing moments (Nm)
D	Disc diameter (m)	p,q,r	Rates of roll, pitch, yaw (rad s^{-1})
L	Lift (N)	x,y,z	Roll, pitch, yaw axes
R	Disc radius (m)	Ω	Spin rate (Hz)

1 INTRODUCTION

In its simplest form a disc-wing can be described as an axi-symmetric wing, most commonly encountered as a Frisbee™ sports disc or a Discus in field athletics. The disc considered in this study has an approximate elliptical cross-section and hollowed out underside cavity i.e. a Frisbee-like configuration. This shape offers interesting possibilities for the development of a small, highly maneuverable unmanned air vehicle (UAV) or projectile of similar description. As a solution to the problem of controlling the disc in flight, it is proposed that flow control methods will be used to modify the aerodynamic forces and moments rather than conventional moving surfaces. Flow control methods such as the placement of vortex generators or synthetic (massless) jets [7] on the leading edge rim to delay the initial boundary layer separation. This paper describes the flow visualisation techniques used to identify suitable surface regions for the effective implementation of fluid control methodologies.

As an introduction to the dynamics of disc-wing flight consider Fig. 1a. Note that for a Frisbee-like shape at typical flight angles of attack, the centre of pressure of the disc-wing is ahead

Authors: *[1]Fluid Mechanics Research Group, The Manchester School of Engineering, The University of Manchester, Oxford Road, Manchester, M13 9PL, U.K.*
[2]Lecturer, Division of Aerospace Engineering, The Manchester School of Engineering, The University of Manchester, Oxford Road, Manchester, M13 9PL, U.K.

Corresponding author: Jonathan R. Potts (e-mail: jonp@fs1.ae.man.ac.uk)

of the centre of the disc i.e. ahead of the disc cg. This results in an untrimmed nose up pitching moment. If the disc is rotating, gyroscopic effects dictate that this pitching moment results in a precessional rolling rate, p. Thus spin provides enhanced pitch stiffness at the expense of roll stability. Using the conventional body fixed axes definition (Fig 1b), for a disc rotating in the direction of positive yaw then a positive pitching moment will generate a negative roll rate.

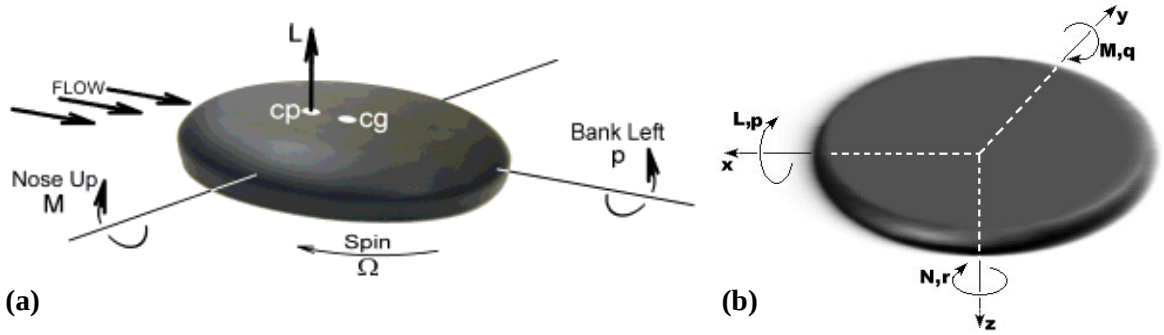

Fig. 1. (a) Disc-wing flight dynamics. (b) Schematic diagram of body fixed axes.

Disc-wing aerodynamics have been studied by a number of researchers in the past. The U.S. Navy commissioned a project to further the development of a self-suspended flare, which was essentially a rotating disc-wing. Stilley & Carstens (1972) investigated the aerodynamics of the flare and other similar disc-wings [1,2]. Nakamura & Fukamachi (1991) visualised the flow past a Frisbee™ using the smoke wire method [3]. Zdravkovich et al. (1998) studied the aerodynamics of a 'coin-like cylinder' disc-wing [4]. Potts & Crowther (2000) investigated the aerodynamic loads of an identical disc-wing [5] to the one in the present work. The results were in reasonable agreement with Stilley & Carstens [1,2] for a similarly shaped disc-wing.

This paper presents results obtained using surface paint and smoke wire flow visualisation techniques. This provides visual evidence for the identification of flow structures associated with the disc-wing flow field and enabled a full description of the flow regime in the vicinity of the disc. A brief outline of the aerodynamic forces and moments acting on a rotating disc-wing is given also. Details of the experimental methods used, together with the results are presented and discussed with reference to previous work on coin-like cylinders and disc-wings. The disc-wing flow topology is proposed based upon surface flow patterns and smoke filament observations.

2 EXPERIMENTAL METHODS

2.1 Wind Tunnels & Apparatus

The disc-wing was tested in two low speed wind tunnels: The first had an open-circuit with a test section of 0.9×1.1m, a top speed of 50m/s and a turbulence level of 0.5%. The second wind tunnel had a closed-circuit with a test section of 2.1×2.7m, a top speed of 70m/s and a turbulence level of 0.1%. The second tunnel was used for the smoke wire experiments due to the superior flow quality at very low speeds.

A number of metal frames were used to mount the disc-wing in the wind tunnel in various configurations. The first (Fig. 2a) was an L shaped arm with the disc mounted vertically on a horizontal axle supported by a vertical strut. The second (Fig. 2b) was used for flow visualisation and held the disc in the horizontal plane.

The disc-wing cross-sectional profile can be seen in Fig. 3. The aspect ratio, *AR*, for a circular planform is $4/\pi \approx 1.27$. For the discs tested, the centre line thickness to chord ratio T/D was 0.14.

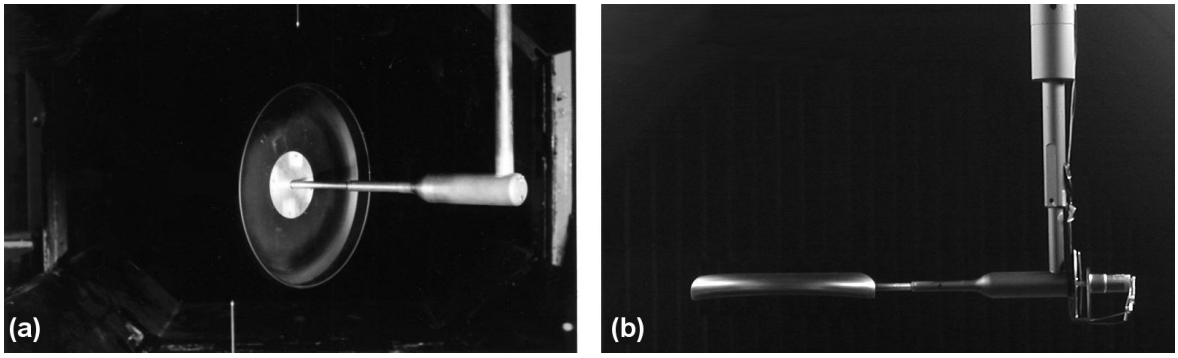

Fig. 2. The L-shaped rig configuration supporting:
(a) a vertical disc-wing at incidence, (b) a horizontal disc-wing at zero incidence

A number of disc-wing models were used for the testing, the first was an aluminium disc and the others were produced from a plastic injection mold. The profile, dimensions and T/D of all these discs matched that of Fig. 3, D = 0.275m.

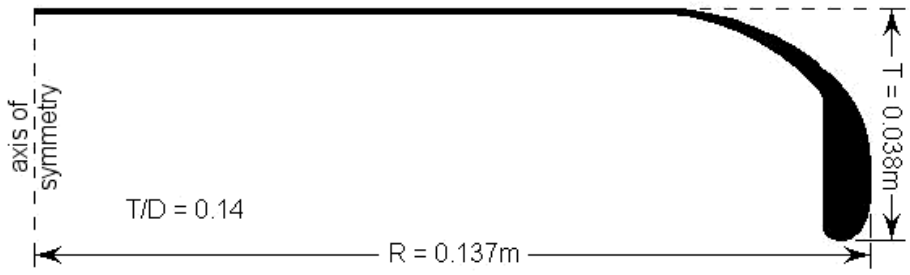

Fig. 3. Cross-sectional disc-wing profile.

2.3 Force and Moment Data

The disc-wing was tested over a speed range of 6m/s to 20m/s, corresponding to a range of Reynolds numbers from 1.13×10^5 to 3.78×10^5. The balance was yawed to vary the incidence through a test range of -10° to 30° and various spin rates were tested up to an advance ratio of 1. Interference and tare effects due to the strut were measured using a dummy support.

2.4 Surface Flow Visualisation

Various methods for surface flow visualisation include fluorescent paints, minitufts and more recently shear sensitive crystals. Fluorescent paints were used for this investigation as this technique fixes the surface flow patterns, which allows the disc to be photographed outside the wind tunnel. Different solutions of paint powder/thinner are used for this technique such as talcum powder/paraffin [4], the ratio of each mixed as desired. The solution is applied to the body surface and mounted in the wind tunnel until the flow patterns are fixed as the paint dries out. The streak lines in the paint display the time-averaged orientation of the surface flow direction and reveal important surface flow structures, such as separation lines. This technique is impractical for a spinning disc.

A film of fluorescent paint, made up of a mix of two parts kerosene to one part fluorescent powder, was applied liberally to the surface of a non-spinning disc-wing. The disc was then placed in the wind tunnel mounted in the horizontal plane (0° incidence), this limited surface drips from interfering with the surface flow patterns. As the kerosene evaporated the time-averaged surface flow patterns were revealed. The resulting patterns were photographed with a digital camera under ultra-violet rich lighting. Surface paint patterns were produced for the flow over both the upper and cavity surfaces from 0° to 30° incidence, V = 15m/s.

2.5 Smoke Wire Flow Visualisation

There are many methods for generating smoke filaments such as the smoke wire, smoke wand and smoke rake. The smoke wire technique was chosen for this investigation as it could provide many thin smoke filaments, ideal for the visualisation of a complex 3D flow such as this. The smoke is generated by the resistive heating of a wire causing the vapourisation of oil droplets. As the flow passes the wire it creates a smoke filled wake behind it. With a small diameter wire (0.1mm) and at low speeds (<2m/s) the wake is laminar, producing clearly defined smoke filaments. The most rewarding results from the smoke wire technique are achieved by a careful balance of flow speed, electrical power and oil supply. As with any other flow visualisation technique the captured images are only as good as the camera and lighting equipment.

A vertical wire was mounted upstream of the disc with a pressurised oil reservoir connected allowing continuous feed (Fig. 4). The nichrome flat wire (0.1×0.4mm rectangular cross-section) was electrically heated causing the oil to vaporise producing smoke filaments. The wire was aligned with the flow so that the narrow edge pointed upstream, this limited the turbulence generated behind the wire. A number of models were constructed so that the disc-wing could be mounted in both the vertical and horizontal planes. This allowed the wire to remain vertical and therefore continuous smoke filaments could be generated due to the gravity oil feed system. The disc was tested at a maximum flow speed of 3m/s and 0° to 50° incidence. At speeds greater than 3m/s smoke filaments from the wire became turbulent.

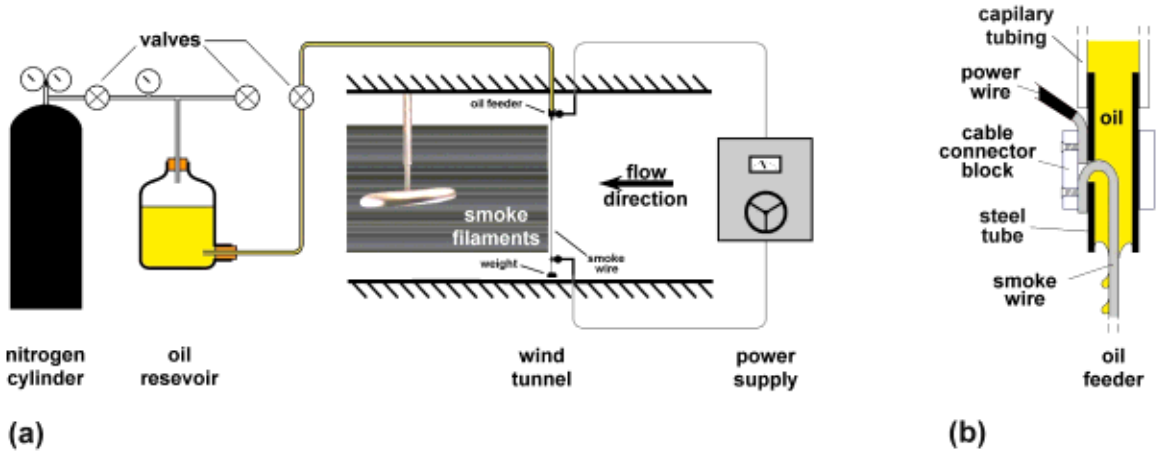

Fig. 4. Schematic diagram of (a) the smoke wire and oil supply system, (b) the oil feeder device

An oil feed system (Fig. 4a) was set up on the wind tunnel to provide a continuous supply to the smoke wire. A regulated cylinder filled with compressed nitrogen pressurised an oil reservoir to 10psi, this was held above the tunnel. The reservoir pressure forced the oil to flow along the capillary tubing and dripped oil onto the smoke wire through the feeder device (Fig. 4b). The oil feeder was a simple and effective device that dripped oil onto the wire through a narrow bore steel tube, this also provided a contact for the power supply. The wire was electrically heated by a power supply connected at each end and the base of the wire was weighted to keep it taut.

The flow field cross-sections were illuminated using 1000Watt halogen spot lamps positioned on opposite sides of the disc. The cross-sections of the separation and vortex structures were illuminated using a laser light sheet. The laser beam was transmitted through a fibre optic cable and a cylindrical lens split the beam into a light sheet of 4mm thickness. The air-cooled, argon-ion laser was operated at 200mW intensity. Footage of the smoke was captured by a video camera operating at various shutter speeds and individual images were transferred to a computer via a frame grabber card. For optimum image definition and contrast, Ondina oil was chosen as it generates clearly visible smoke filaments.

3 EXPERIMENTAL RESULTS AND DISCUSSION

3.1 Force and Moment Data

The aerodynamic forces and moments acting on the disc-wing are dependent upon speed, rotation rate and angle of attack. The loads were measured for the range of conditions that the disc-wing will experience in free flight. Over an angle of attack range of -10° to 30°, the lift curve is linear whereas the drag curve is parabolic. These results are consistent with what would be expected for a typical low aspect ratio wing. The pitching moment curve is non-linear and the rolling moment is essentially zero, which is expected for a symmetrical body. The effect of spin is small but measurable, most significantly causing a non-zero 'Magnus rolling moment' [1,2]. The reader is referred to Potts & Crowther [5] for a detailed analysis of the aerodynamic load data.

3.2 Surface Flow Visualisation

Visualisation of the flow over the upper and lower surfaces of the disc at zero angle of attack is shown in Fig. 5. The upper surface pattern (Fig. 5a) shows that the surface flow direction is from the leading edge towards L_1, indicated by the streak lines within region A. The boundary layer separates from the surface leaving a clearly visible line (L_1) and the shear layer reattaches at L_2. The boundary layer remains attached throughout region C and then separates off the surface at L_3. A separation bubble is formed with reversed flow (from L_2 to L_1) on the surface and re-circulation within region B. From the trailing edge, a reversed surface flow pattern is observed within region D, as fluid is drawn towards the stagnation line at L_3. Two nodes at the points V_1,V_2 indicate where trailing vortices detach from the surface. Streak lines in the vicinity of V_1,V_2 suggest that fluid from the separation bubble and from beneath the cavity feeds into these vortices.

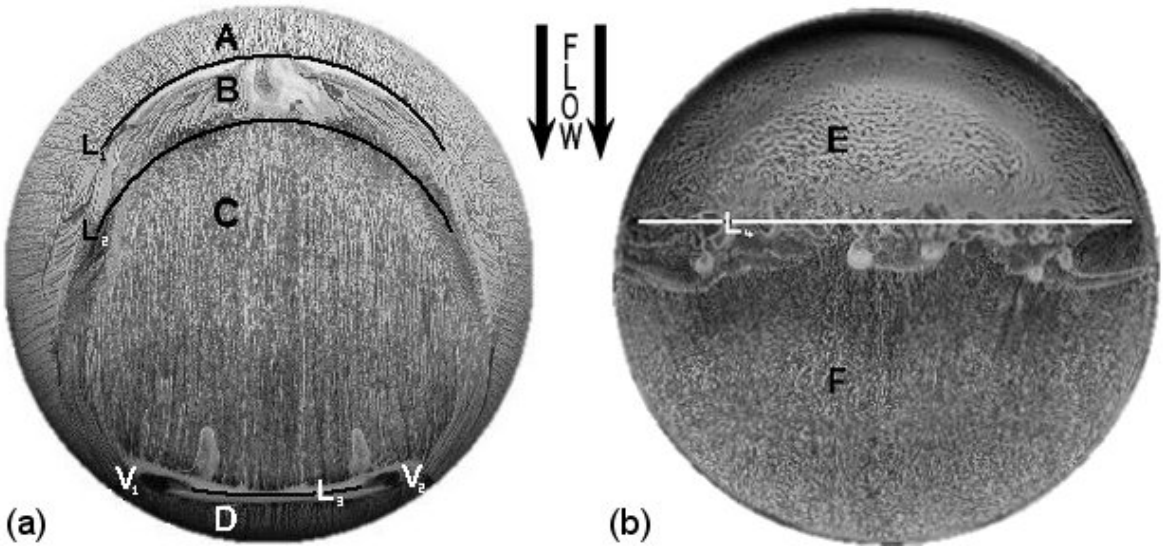

Fig. 5. The upper (a) and cavity (b) surface paint patterns at 5° incidence, 15m/s.

The general description of the cavity surface flow is given with reference to Fig. 5b. The cavity surface pattern indicates that the boundary layer separates off the leading edge lip and impinges on the inside of the trailing edge rim leaving a stagnation line (which cannot be seen on Fig. 5b). Reversed flow (F) exists from the trailing edge towards the stagnation line L_4. The shear layer encloses a weakly circulating separation bubble (E).

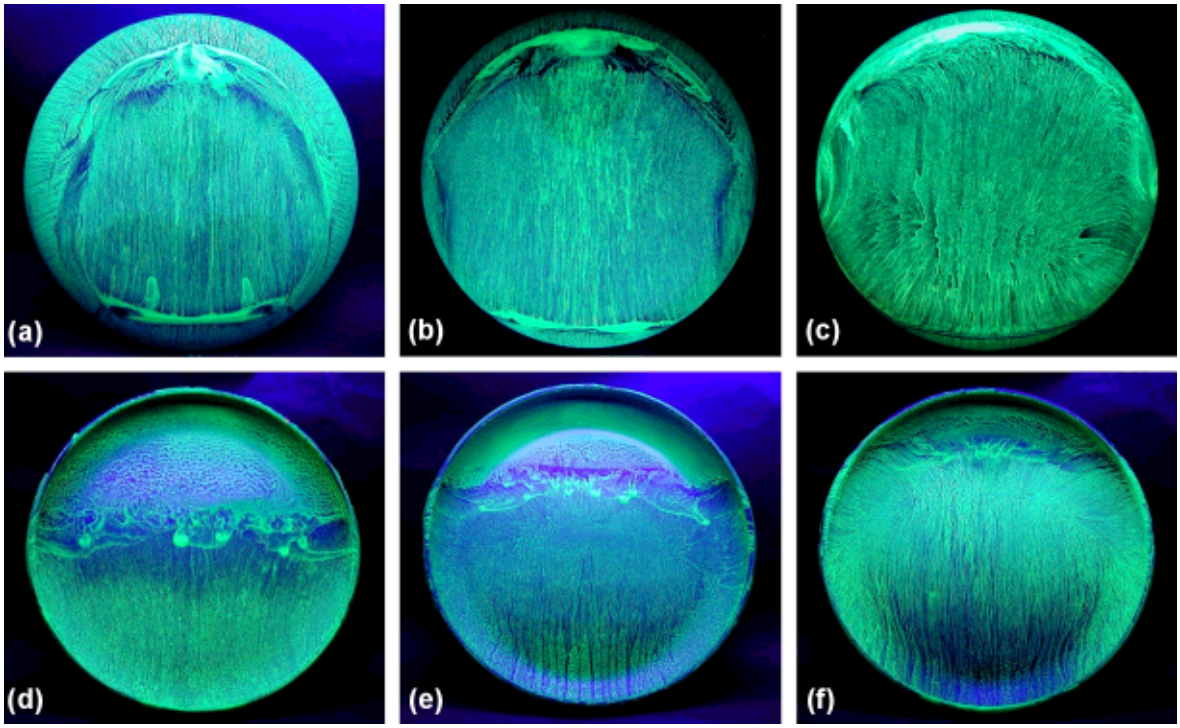

Fig. 6. Upper (a,b,c) and cavity (d,e,f) surface paint flow visualisation patterns at 5° (a,d), 15° (b,e) & 25°(c,f) incidence, V = 15m/s.

The variation of upper surface flow patterns with incidence is shown in Fig. 6a-c. The flow separates at an arc of constant radius throughout the incidence range 0° to 30°, the position of the separation line moving upstream with incidence. The separated boundary layer reattaches at an arc of constant radius for the range 0° to 10° incidence. The unsteady stagnation line, of reattachment, moves downstream with increased incidence and becomes straight (15°). This is difficult to see on Fig. 6 but it is possible to see the average stagnation line for 20° incidence on Fig. 7a. The arrows show the flow direction away from the line. As this stagnation line travels further downstream it narrows towards becoming a nodal point (Fig. 7b). This radial outflow has left an uneven pattern suggesting unsteady effects as the shear layer dictates the surface flow in this locality. The trailing edge stagnation line exists between the detachment of two trailing vortices V_1,V_2 at symmetrical positions for 0° to 10° incidence. These vortices move upstream with increased incidence around the circumference of the disc.

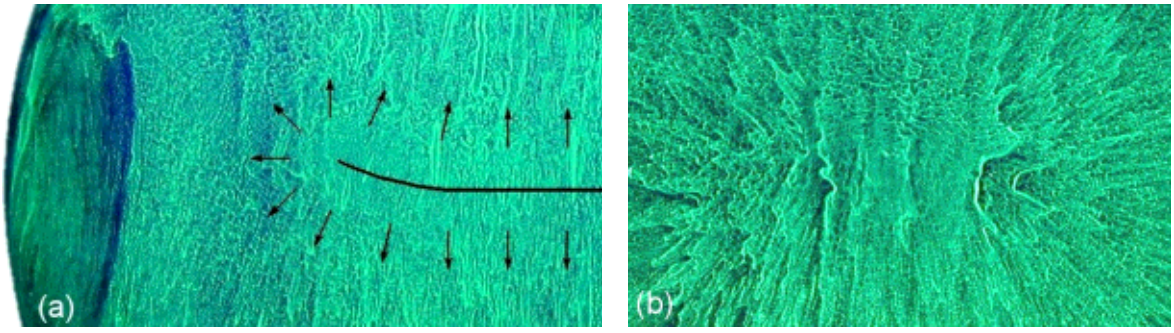

Fig. 7. (a) The time-averaged stagnation line (half disc) on the upper surface paint pattern at 20° incidence, V = 15m/s. (b) The stagnation line/nodal point on the upper surface paint pattern at 30° incidence, V = 15m/s.

The variation of cavity surface flow patterns with incidence is shown in Fig. 6d-f. The shear layer separates off the leading edge lip and reattaches inside the trailing edge rim for 0° to 10° incidence. For increased incidence this reattachment line moves upstream and becomes straight (15°). Reversed flow on the surface occurs ahead of the reattachment, the recirculation has formed a stagnation line which is straight at 5° incidence and moves upstream with increased incidence. The flow upstream of this stagnation line has not disturbed the surface paint much, observations of the paint patterns show reversed surface flow but the flow here would be better described as stagnant. At increased incidence (15°+) the reattachment moves upstream of the centre of the disc and the flow is attached to the trailing edge rim before it separates at the trailing edge lip. Between the reattachment and stagnation for 15° incidence the reversed flow creates a narrow strip on the surface which suggests the possible formation of a vortex filament. It is also worth noting that, on the downstream half of the cavity, the streak lines aft of the reattachment can be seen to converge on the centre line, particularly for higher incidence. This is due to the convergence of fluid within the cavity as the rim narrows towards the trailing edge.

3.3 Smoke Wire Flow Visualisation

Results from smoke wire flow visualisation have revealed information regarding the flow field particularly the separation bubble and trailing vortices. The central cross-section of the flow field over a non-rotating disc-wing at various angles of attack are shown in Fig. 8. At 0° incidence (Fig. 8a) the flow field shows straight smoke filaments which are relatively undisturbed from their free-stream shape, except for the turbulent bluff body wake. As incidence increases to 10°,20° the filaments show upward deflection upstream of the leading edge and subsequent downwash aft of the trailing edge. At 30°,40° incidence the curvature of the filaments is particularly apparent (Fig. 8d,e) as is the vortex shedding off the trailing edge in the wake of the disc. The separation bubble is visible as a dark region close to the leading edge, the smoke was not entrained into the structure but the separated shear layer outlines the shape. The shear layer reattaches to the surface on the centre line throughout the range 0° to 40° incidence, full separation occurs at 45° creating a wider wake shedding larger vortex structures, see Fig.10f with the wing in deep stall.

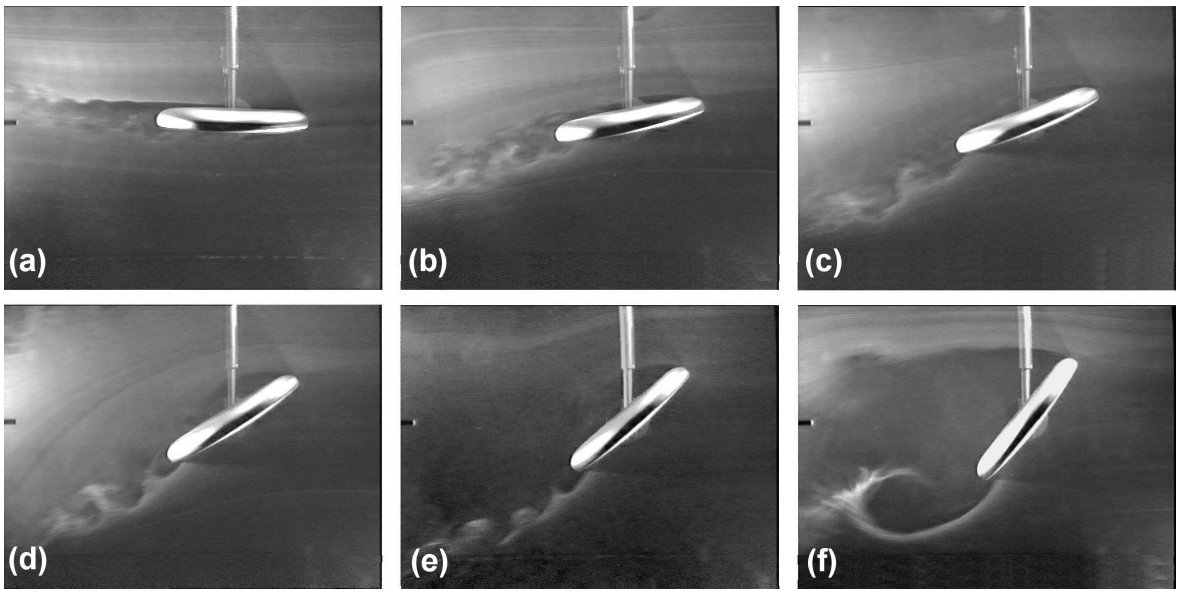

Fig. 8. Central cross-section of the flow field over a non-rotating disc-wing at (a) 0°, (b) 10°, (c) 20°, (d) 30°, (e) 40° & (f) 50° incidence, V = 3m/s.

The central cross-section of the separation bubble at various angles of attack is shown in Fig. 9, illuminated by a laser light sheet. The laminar separation forms a distinct shear layer and the unsteady reattachment entrains smoke into the bubble. The separated shear layer is seen to become unstable due to a similar process to the Kelvin-Helmholtz instability for inviscid flows, according to linear stability theory. The shear layer rolls up into one or more laminar structures before becoming turbulent. The separation bubble forms even at zero incidence (Fig. 9a), the thickness of which enlarges with increased incidence. It is possible to see the reattachment of the shear layer in Fig. 9a where a slug flattens out on the surface and reaches into the separation bubble. Whilst observing the separation bubble in the wind tunnel the reattachment was seen to dance on the surface in an unsteady manner. Note the upwash angle of the fluid upstream of the leading edge.

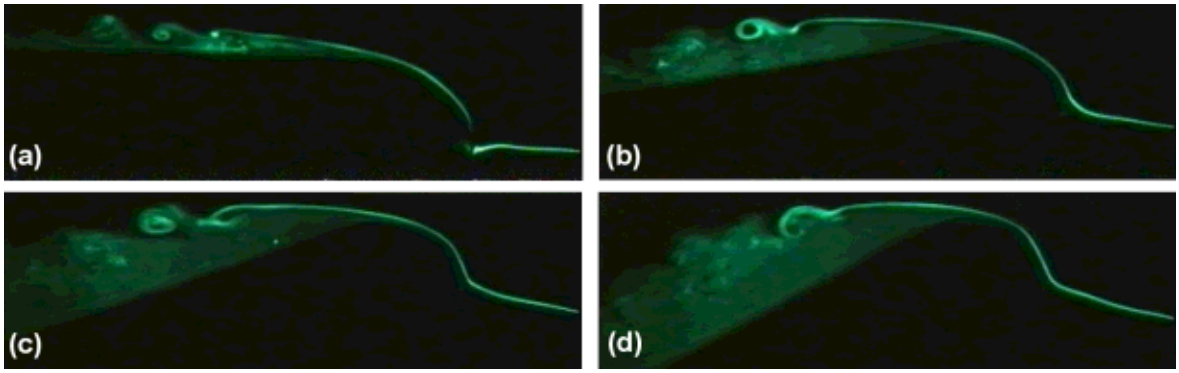

Fig. 9. Central cross-section of the separation bubble over a disc-wing at (a) 0°, (b) 10°, (c) 20° & (d) 30° incidence, AdvR = 0.7, V = 3m/s

A cross-section of the bluff body wake/trailing vortices is shown at various angles of attack in Fig. 10, illuminated by a laser light sheet. The cross-section seen in Fig.10a shows little vorticity at 0° incidence, a turbulent bluff body wake exhibited here. As the incidence increases the central downwash develops and more rotation is given to the trailing vortices. The structure of the trailing vortices begins to develop at 5° incidence (Fig. 10b) but the turbulence generated by the bluff body still visible. At 10° incidence the vortex structures are much better defined (Fig. 10c).

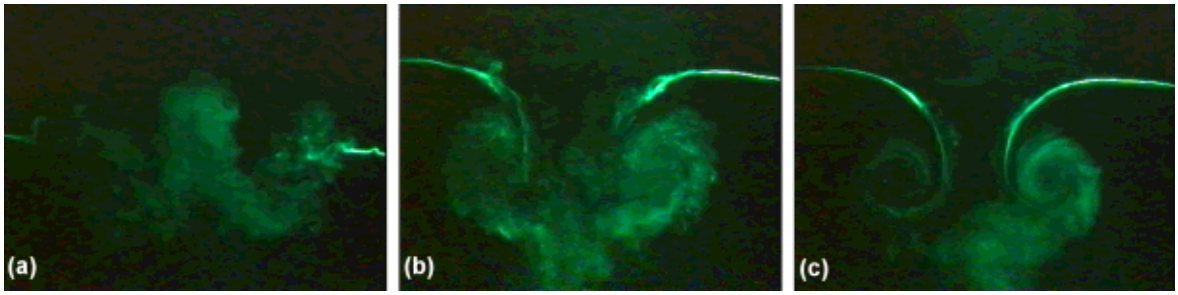

Fig. 10. Cross-section of the wake downstream from a non-rotating disc-wing at a distance of one diameter from the trailing edge at (a) 0°, (b) 5°& (c) 10° incidence, V = 3m/s

The central cross-section of the cavity separation at 10° incidence is shown in Fig. 11, illuminated by a laser light sheet. The laminar separation on the leading edge lip forms a distinct shear layer (Fig. 11a) which becomes unstable (Kelvin-Helmholtz instability) rolling up into one or more laminar structures before becoming turbulent. The interaction of these unstable structures generated by the shear layer is captured in Fig. 11b. The turbulent recirculation within the cavity stems from the trailing edge rim with reversed flow observed beneath the shear layer.

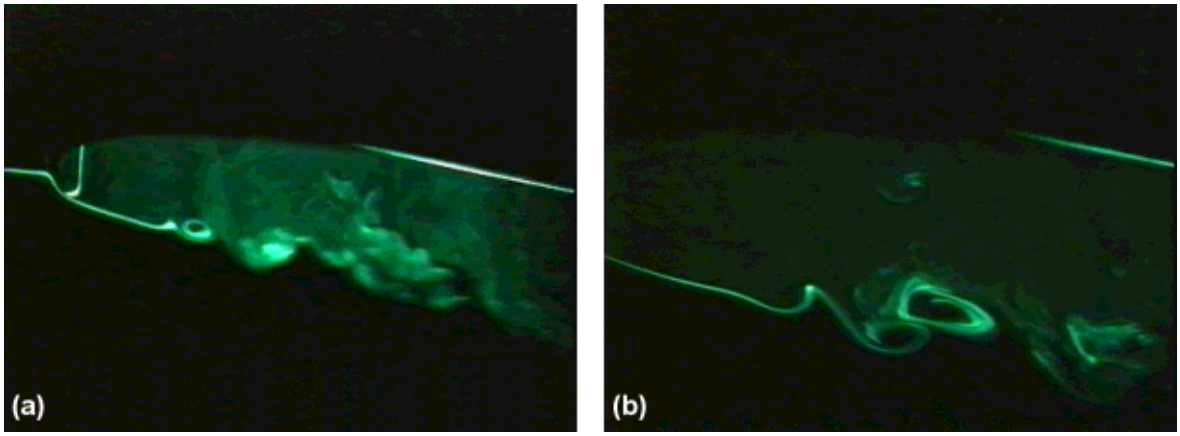

Fig. 11. Central cross-section (a) and close up (b) of the separated shear layer and cavity flow over a non-rotating disc-wing at 10° incidence, V = 3m/s.

3.4 Proposed Disc-wing Flow Topology

The proposed topology of the flow over a non-rotating disc-wing is given based upon surface flow patterns and smoke filament flow visualisation. The two-dimensional flow cross-section shown in Fig. 12a depicts many of the flow structures that have been previously discussed. In addition, the reattachment point of the cavity shear layer can be seen on the inside of the trailing edge rim. From the stagnation point on the trailing edge lip, the surface flow was drawn up the back of the trailing edge rim, towards another stagnation point at the top of the rim. This was seen as reversed flow on the upper surface patterns.

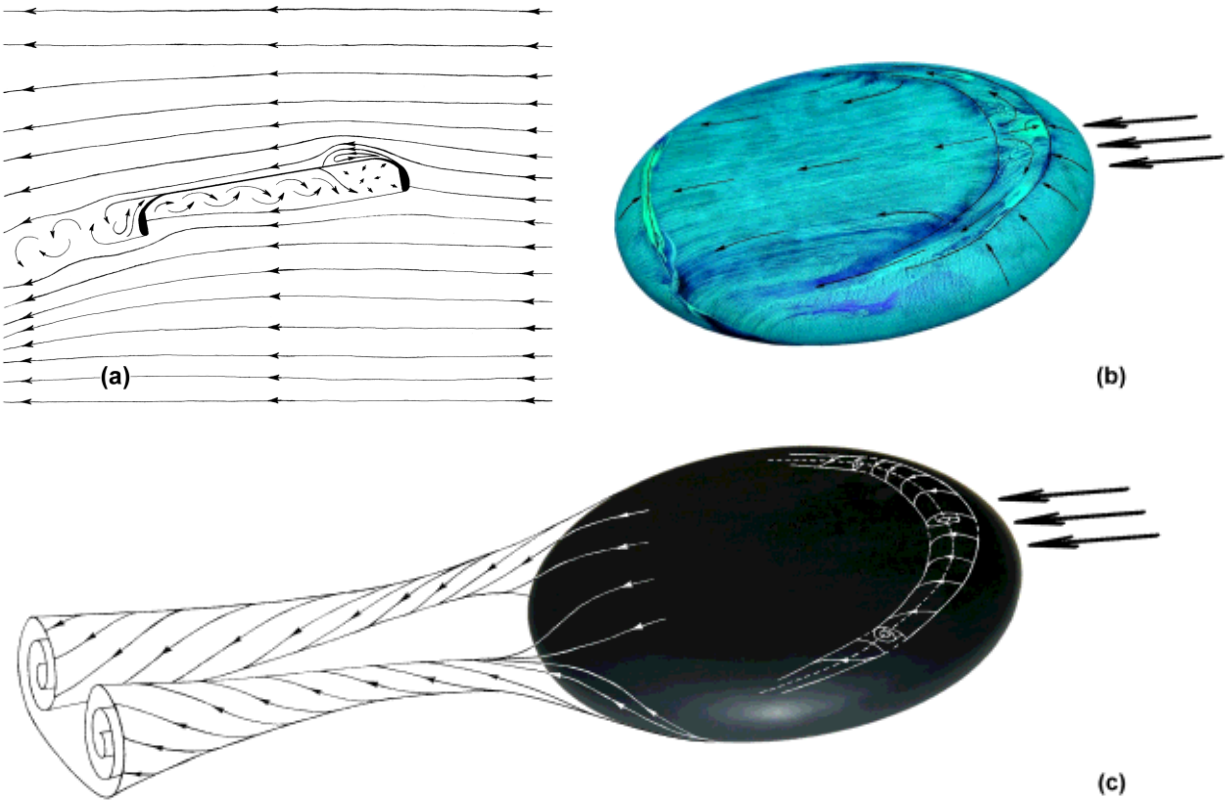

Fig. 12. Flow topology and upper surface pattern for a non-rotating disc-wing at 10° incidence (a) 2D central cross-section (b) 3D surface flow (c) 3D trailing vortices & separation bubble

The three-dimensional flow topology shown in Fig. 12b,c depicts many of the flow structures previously described. In addition, there is reversed flow on the surface within the separation bubble towards a central node of separation (Fig. 12b). The trailing vortices (Fig 12c) move closer to each other initially as they detach from the surface before diffusing in the usual way, vorticity in the direction shown.

4 CONCLUSIONS

The upper surface flow is characterised by an arc separation line on the leading edge rim, followed by an arc shaped reattachment. The cavity flow is characterised by separation at the leading edge lip and reattachment inside the trailing edge rim. Reversed flow occurs within the cavity forming a straight stagnation line.

The separation bubble is enclosed by a laminar shear layer which becomes unstable, the unsteady reattachment is observable and entrains fluid into the recirculating structure. The trailing vortices detach from the trailing edge rim, they are close together creating a strong central downwash which causes the flow to reattach at high incidence.

The combination of flow visualisation techniques used in the present study, were necessary to gather enough information for the effective implementation of a fluid control method. Fluorescent paints have defined the separation and reattachment lines for a non-rotating disc. The smoke wire technique has shown that there is little difference between the surface flow regime for rotating and non-rotating discs, although small asymmetries have been observed with rotation.

ACKNOWLEDGEMENTS

The authors would like to thank D. Mould for the skilled construction of the rig & disc and I. Lunnon for the smart design of the oil feeder, both based at the Goldstein Research Laboratory. This research was funded by the EPSRC, award reference number 98317373.

REFERENCES

[1] Stilley G.D. and Carstens D.L.: Adaptation of frisbee flight principle to delivery of special ordnance. *AIAA 2nd Atmospheric Flight Mechanics Conference*, Palo Alto, California, USA, AIAA Paper No. 72-982, 1972.

[2] Stilley G.D.: Aerodynamic analysis of the self-suspended flare. Honeywell Inc., NAD/Crane RDTR No.199, AD740117, 23 Feb. 1972.

[3] Nakamura Y. and Fukamachi N.: Visualization of the flow past a frisbee. *Fluid Dyn. Res.*, Vol. 7, pp 31-35, 1991.

[4] Zdravkovich M.M., Flaherty A.J., Pahle M.G. and Skelhorne I.A.: Some aerodynamic aspects of coin-like cylinders, *J. Fluid Mech.*, Vol. 360, pp 73-84, 1998.

[5] Potts J.R. and Crowther W.J.: The flow over a rotating disc-wing. *RAeS Aerodynamics Research Conference Proc.*, London, UK, Apr. 2000.

[6] Tobak M. and Peake D.J.: Topology of three-dimensional separated flows, *Ann. Rev. Fluid Mech.*, Vol. 4, pp61-85, 1982.

[7] Crook A. and Wood N.J.: A parametric investigation of a synthetic jet in quiescent conditions. *Proc. of the Ninth International Symposium on Flow Visualization*, Edinburgh, Scotland, UK, 2000.

[8] Mueller T.J.: Recent developments in smoke flow visualization. *Proc. of the Third International Symposium on Flow Visualization*, Ann Arbor, Michigan, USA, 1983.